Four Tilting Rotor Convertible MAV: Modeling and Real-Time Hover Flight Control

Gerardo Ramon Flores Colunga, Juan Antonio Escareño, Rogelio Lozano, Sergio Salazar

myjournal manuscript No.
(will be inserted by the editor)

Four Tilting Rotor Convertible MAV:

Modeling, Control and Real-time Hover Flight Control

G. Flores[1], J. Escareño[1], R. Lozano[1], S. Salazar[2]

[1] Heudiasyc, UTC, CNRS 6599, 60205 Compiègne, France
[2] French-Mexican Laboratory on Computer Science and Control, CINVESTAV, Mexico City

Received: 16 Feb 2011 / Revised version: 02 Apr 2011

Abstract This paper describes the modeling, control and hardware implementation of an experimental tilt-rotor aircraft. This vehicle combines the high-speed cruise capabilities of a conventional airplane with the hovering capabilities of a helicopter by tilting their four rotors. Changing between cruise and hover flight modes in mid-air is referred to transition. Dynamic model of the vehicle is derived both for vertical and horizontal flight modes using Newtonian approach. A nonlinear control strategy is presented and evaluated at simulation level to control, the vertical and horizontal flight dynamics of the vehicle in the longitudinal plane. An experimental Quad-plane aircraft was developed to perform the vertical flight. A low-cost DSP-based Embedded Flight Control System (EFCS) was designed and built to achieve autonomous attitude-stabilized flight.

1 Introduction

The applications of mini Unmanned Aerial Vehicles (UAVs) have widely diversified during the last years. They comprise both military and civilian, though the latter has had a lower development rate. The key feature of UAVs is to provide a mobile extension of human perceptions allowing not only the security of the user (soldier, policeman, cameraman, volcanologist) but also gathering information such as images or video, locations coordinates, weather conditions, etc., for either online or offline analysis. As a result, the use of aerial robots, specially miniature (mini and micro) UAVs (MAVs), has

Send offprint requests to: G. Flores
Université de Technologie de Compiègne
Tel.: +33 44 23 44 23
E-mail: gfloresc@hds.utc.fr

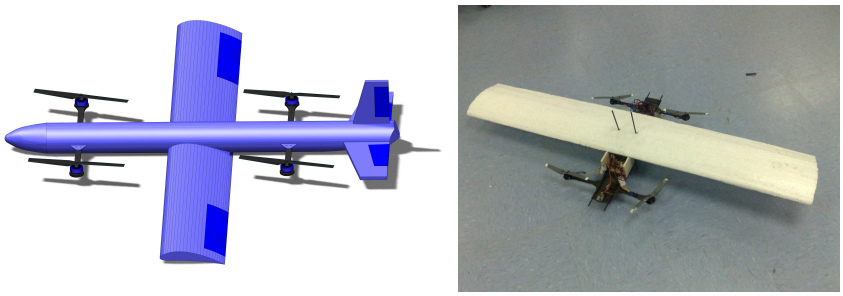

(a) CAD. (b) Experimental prototype.

Figure 1 Quad-Tilting Rotor Convertible UAV.

enhanced activities such as surveillance of sensible areas (borders, harbors, prisons), wildlife study, natural disasters assessment, traffic surveillance, pollution monitoring, just to mention a few.

However, there are missions whose scope is beyond the capabilities of conventional small UAVs designs since they require not only longer flight endurance but also hovering/VTOL capabilities.

Missions like the surveillance of both fast-moving and static targets, identification of cracks in pipelines or bridges, medical supplies (blood samples, saliva samples, medications) exchange between hospitals and clinics located in remote areas, are missions which can not be acomplished with standard airplanes or helicopters. Besides these commonly used aerial vehicles, the Hybrid or Convertible MAVs, combining the advantages of horizontal and vertical flight, have been gaining popularity recently. By marrying the take-off and landing capabilities of the helicopter with the forward flight efficiencies of fixed-wing aircraft, the Quad-plane promises a unique blend of capabilities at lower cost than other UAV configurations. While the tilt-rotor concept is very promising, it also comes with significant challenges. Indeed it is necessary to design controllers that will work over the complete flight envelope of the vehicle: from low-speed vertical flight through high-speed forward flight. The main change in this respect (besides understanding the detailed aerodynamics) is the large variation in the vehicle dynamics between these two different flight regimes. Several experimental platforms have been realized with a body structure in which the transition flight is executed by turning the complete body of the aircraft [4], [5], [1], [3], [2]. In [1] and [3] the authors described the development (modeling, control architecture and experimental prototype) of Two-rotor tailsitter. The control architecture features a complex switching logic of classical linear controllers to deal with the vertical, transition and forward flight. [4] presents a classical airplane configuration MAV to perform both operational modes. The hover flight is autonomously controlled by an onboard control flight system while the transition and cruise flight is manually controlled. A standard

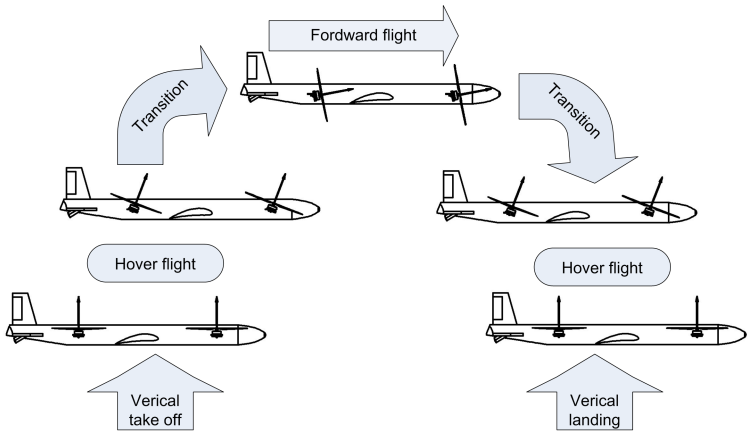

Figure 2 Operational transition.

PD controller is employed during hover flight to command the rudder and elevator. In [5] some preliminary results are presented for the vertical flight of a Two-rotor MAV as well as a low-cost embedded flight control system. There are some examples to other tilt-rotor vehicles with quad-rotor configurations like Boeing's V44 [9] and the QTW UAV [10]. In [11] the authors present the progress of their ongoing project, an aircraft with four tilting wings.

This paper reports current work on the modeling, control and development of an experimental prototype of a new tilt-rotor aircraft (Quad-plane Unmanned Aerial Vehicle) that is capable of flying in horizontal and vertical modes. The vehicle is driven by four rotors and has a conventional airplane-like structure, which constitutes a highly nonlinear plant and thus the control design should take into account this aspect. A nonlinear control strategy, consisting of a feedback-linearizable input for altitude control and a hierarchical control (inner-outer loop) scheme for the underactuated dynamic subsystem (x-position, pitch), is proposed to stabilize the aerial robot within the hovering mode. This mini aerial vehicle is one of the first of its kind among tilt-wing vehicles on that scale range.

The organization of this paper is as follows: in Section II, the mathematical model of the Quad-plane aircraft is obtained using the Newton formulation. In Section III, we explain how the transition flight is developed and how the velocities, forces and angles they interact. In Section IV, we develop a stabilizing control law for the vehicle in hover flight mode. In Section V, we present a backstepping control law for the vehicle in forward flight mode. Simulation results of both controllers are presented in Section VI. Experimental results are provided in Section VII. Conclusions and perspective are provided in Section VII and Section VIII, respectively.

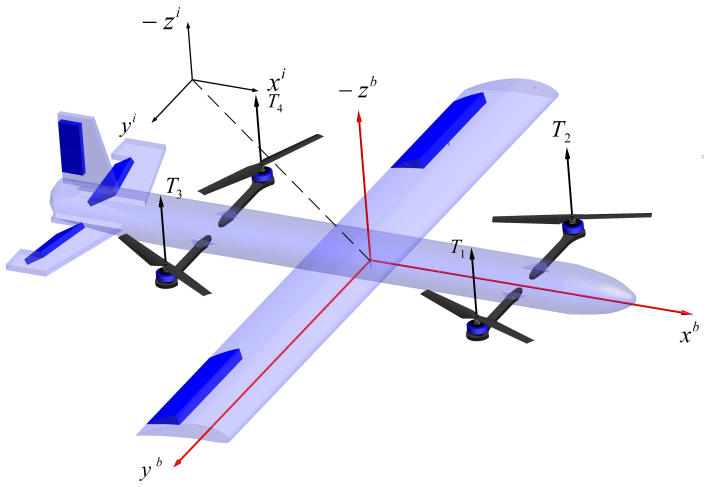

Figure 3 Coordinate systems: Inertial frame (F^i) and Body-fixed frame (F^b)

2 Modeling

This section presents the longitudinal equations of motion as well as the aerodynamics of the vehicle. Due to the flight profile of the vehicle we distinguish three operation modes: (1) *Hover Flight (HV)* the aircraft behaves as a rotary-wing platform ($|\gamma| \leq \frac{\pi}{6}$), (2) *Slow-Forward Flight (SFF)* ($\frac{\pi}{6} < |\gamma| \leq \frac{\pi}{3}$) and finally (3) *Fast-Forward Flight (FFF)*, where the aerial robot behaves as a pure airborne vehicle ($\frac{\pi}{3} < |\gamma| < \frac{\pi}{2}$).

1. During the *HF* the 3D vehicle's motion relies only on the rotors. Within this phase the vehicle features VTOL flight profile. The controller for this regime disregard the aerodynamic terms due to the negligible translational speed.
2. It is possible to distinguish an intermediate operation mode, the SFF, which links the two flight conditions, *HF* and *FFF*. This is probably the most complex dynamics.
3. *FFF* regime mode (Aft position), at this flight mode the aircraft has gained enough speed to generate aerodynamic forces to lift and control the vehicle motion.

2.1 Kinematics

– $\mathcal{F}^i$ denotes the inertial earth-fixed frame with origin, O^i, at the earth surface. This frame is associated to the vector basis $\{i_i, j_i, k_i\}$.
– $\mathcal{F}^b$ denotes the body-fixed frame, with origin, O^b, at the center of gravity CG. This frame is associated to the vector basis $\{i_b, j_b, k_b\}$.

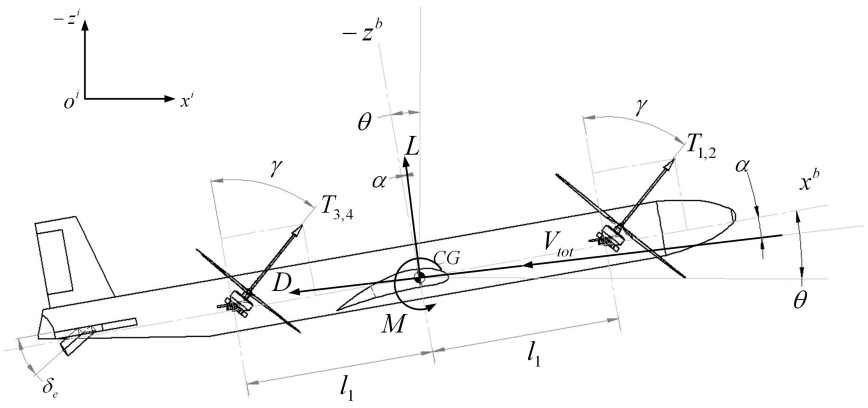

Figure 4 Free-body scheme showing the forces acting on the Quad-tilting MAV.

- $\mathcal{F}^a$ denotes the aerodynamic frame, with origin, O^b, at the center of gravity CG. This frame is associated to the vector basis $\{i_a, j_a, k_a\}$.
- The orthonormal transformation matrices $\mathcal{R}^{bi}$ and $\mathcal{R}^{ab}$, respectively used to transform a vector from $\mathcal{F}^b \rightarrow \mathcal{F}^i$ and $\mathcal{F}^a \rightarrow \mathcal{F}^b$ within the longitudinal plane (pitch axis), are given by:

$$\mathcal{R}^{bi} = \begin{pmatrix} \cos\theta & 0 & \sin\theta \\ 0 & 1 & 0 \\ -\sin\theta & 0 & \cos\theta \end{pmatrix}, \mathcal{R}^{ab} = \begin{pmatrix} \cos\alpha & 0 & \sin\alpha \\ 0 & 1 & 0 \\ -\sin\alpha & 0 & \cos\alpha \end{pmatrix}$$

2.2 Aerodynamics

It is important to consider these forces properly because they are fundamentally affected by the vehicle's motion and thus they alter the basic dynamics involved. The analysis used in the present paper will be based on a combination of a low-order panel method aerodynamic model coupled with a simple actuator disc model of the flow induced by the propellers. In order to proceed with the aerodynamic analysis, it is worth to mention the following assumptions:

- **A1.** The vehicle is a rigid body, i.e. the felexibility of the aircraft wings or fuselage will be neglected.
- **A2.** Non-varying mass is considered ($\dot{m}(t) = 0$).
- **A3.** The aerodynamic center (AC) and the center of gravity (CG) are coincident.

In order to determine the aerodynamic forces exerted on the vehicle, we need to know both the direction and velocity of the total airflow vector. We can identify three wind vectors acting on the vehicle: the airflow speed

V_p produced by the rotors, the V_b airflow generated by the translational motion of the body (U, W) and a third component due to the external wind (disturbance) V_e, generally unknown. Hence, the total wind vector in the body frame can be written as

$$V_{tot} = V_p(\gamma) + V_b + V_e \tag{1}$$

where $V_{tot} = (v_u, v_w)^T$. The total wind vector V_{tot} experienced by the wing varies depending on the flight mode. Within the *HF* and *SFF* regimes the wing is not washed by the propeller airflow V_p (Fig. 5a), while in the *FFF* mode, it is assumed that the wing is significatively submerged (Fig. 5b) by V_p. Therefore the propeller slipstream V_p is disregarded in *HF* and *SFF*. To include the behavior of V_p in the equations let us introduce the following function

$$\xi(\gamma) = \begin{cases} 0 \; if \; \gamma \leq \frac{\pi}{3} \\ 1 \; if \; \gamma > \frac{\pi}{3} \end{cases} \tag{2}$$

The parallel wind velocity v_u and the normal wind velocity v_w components

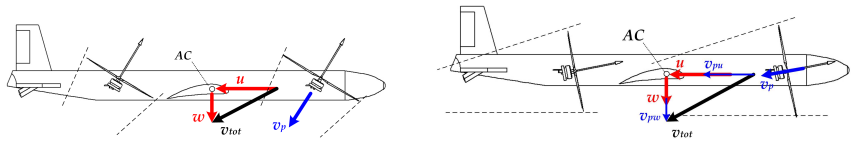

(a) Relative wind velocity in HF and SFF modes

(b) Relative wind velocity in FFF mode

Figure 5 Airflow profile generated by the rotors during the flight envelope

at the wing encompasse the velocity that the vehicle experiments through the air and the corresponding components of V_p due the tilting of the rotors and the aleatory external wind V_e , i.e.

$$V_u = (u + \xi(\gamma) v_p \sin(\gamma) + v_{e_u}) i_b \tag{3}$$

$$V_w = (w + \xi(\gamma) v_p \cos(\gamma) + v_{e_w}) k_b \tag{4}$$

Assuming purely axial flow into the propellers, simple actuator disc theory [13] gives the induced propeller velocity for the i^{th} rotor as

$$v_{p_i} = \sqrt{\frac{2T_i}{\rho A_p}} \tag{5}$$

where A_p is the total disc-area of the propeller and ρ the air density. Figure 4 shows the aerodynamic forces on a small UAV with a tilt angle γ. The

forces consist of a lift force, L, perpendicular to the total flow vector, V_{tot}, a drag force D parallel to V_{tot}, and the airfoil's pitching moment, M, about the positive cartesian y-axis. The above discussion can be summarized by:

$$\begin{aligned} C_l &= C_{l_\alpha}\alpha \\ C_d &= C_{d_p} + C_{d_i} \\ C_m &= C_{m_\alpha}\alpha \end{aligned}$$

where these equations are standard aerodynamic non-dimensional lift, drag and moment coefficients[1] To obtain the lift and drag forces and the pitching moment on the aircraft it is only necessary to obtain the total wind velocity vector V_{tot}, see (1), the angle of attack and the aerodynamic parameters $C_{l_\alpha}, C_{l_\delta}, C_d, C_{m_\delta}, C_{m_\alpha}$ which depend on the geometry of the vehicle.

$$\begin{aligned} L &= \tfrac{1}{2}C_l\rho V_{tot}^2 S \\ D &= \tfrac{1}{2}C_d\rho V_{tot}^2 S \\ M &= \tfrac{1}{2}C_m\rho V_{tot}^2 S\bar{c} \end{aligned}$$

In these equations S and $\bar{c}$ are the area and the wing chord respectively. The angle of attack α and the magnitude of V_{tot} are obtained through the following equations

$$\alpha = \arctan(v_w/v_u) \tag{6}$$

$$V_{tot} = \sqrt{v_w^2 + v_u^2} \tag{7}$$

The lift force will depend on the velocity V_tot and the angle of attack. The following image represents the different values of lift for several speed conditions:

2.3 Forces exerted on the Quad-plane

The vector that contains the set of forces applied to the Quad-plane (Fig. 4) is given by

$$m\ddot{\xi} = \mathcal{R}^{bi}T^b + \mathcal{R}^{bi}\mathcal{R}^{ab}A^a + \mathcal{W}^i \tag{8}$$

where, $\xi = (x, y, z)^T$ is the CG's position vector in $\mathcal{F}^i$, $T^b = (0, 0, -T)^T$ is the collective thrust in $\mathcal{F}^b$, $A^a = (-D, 0, -L)^T$ is the vector of aerodynamic forces in $\mathcal{F}^a$ and finally $\mathcal{W}^i = (0, 0, mg)^T$ denotes the weight of the vehicle in $\mathcal{F}^i$. The four propellers produce the collective thrust T, which can be modeled as

$$T = K_l \sum_{i=1}^{i=4} \omega_i^2 \tag{9}$$

where ω_i is the angular velocity of i^{th}-rotor, K_l is a lift factor depending on the aerodynamic parameters of the propeller. Note that the vector of aerodynamic forces A^a is not only involved in translational motion, but also in the rotational motion of the vehicle, as is shown next.

[1] C_* slopes are obtained from the software XFOIL.

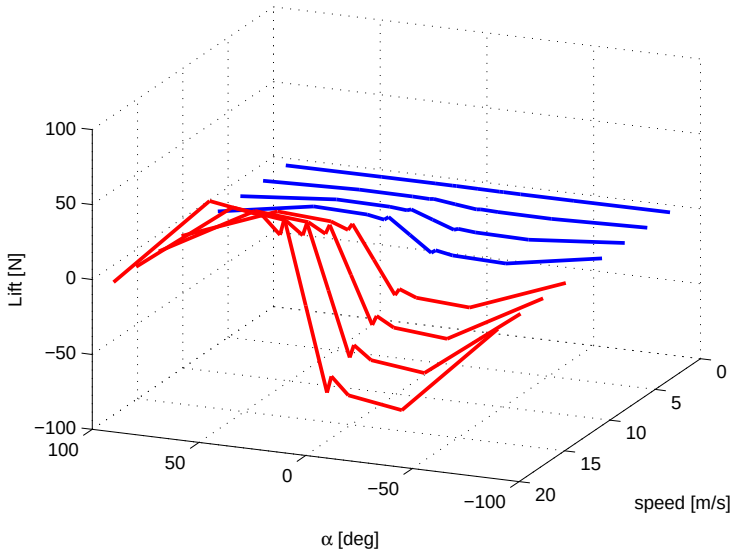

Figure 6 Lift values for different velocities.

2.4 Moments acting on the Quad-plane

The forces shifted away from the center of gravity CG induce moments causing the rotational motion. The corresponding vectorial equation grouping the moments exerted about CG is written as

$$\tau^b = \tau_T^b + \tau_M^b + \tau_G^b \tag{10}$$

where τ_T is the induced moment due the difference of thrust between $T_{3,4}$ and $T_{1,2}$, τ_M is the airfoil's pitching moment, τ_G is the gyroscopic moment. τ_T is obtained through

$$\tau_T^b = l_1(-T_{3,4}\cos\gamma + T_{1,2}\cos\gamma)j_b \tag{11}$$

where, l_1 is the distance from the CG to the rotors. The airfoil's pitching moment τ_M is obtained from the airfoil's C_m slope.

$$\tau_M^b = M\ j_b \tag{12}$$

The gyroscopic moment τ_G arises from the combination of the airframe's angular speed $\Omega^b = (p, q, r)^T$ and the rotors angular speed ω_i. The τ_G vector is then modeled as $\sum_{i=1}^{4}(\Omega^b \times I_p\omega_i)$, leading to

$$\tau_G^b = I_p[q(\omega_2 - \omega_1 + \omega_3 - \omega_4)i_b + p(\omega_1 - \omega_2 - \omega_3 + \omega_4)j_b] \tag{13}$$

where, I_p represents the inertia moment of the propeller. For simplicity we do not take into account the drag torque due to the propeller drag force.

Since the present paper concentrates on the longitudinal flight of the vehicle, the corresponding scalar equations modeling the forces and moments applied to the vehicle are written as:

$$\begin{aligned} m\ddot{X} &= -T_{3,4}\sin(\theta+\gamma) - T_{1,2}\sin(\theta+\gamma) - L\sin(\theta-\alpha) - D\cos(\theta-\alpha) \\ m\ddot{Z} &= D\sin(\theta-\alpha) - T_{1,2}\cos(\theta+\gamma) - L\cos(\theta-\alpha) - T_{3,4}\cos(\theta+\gamma) + g \\ I_{yy}\ddot{\theta} &= M + l_1(-T_{3,4}\cos\gamma + T_{1,2}\cos\gamma) + I_p p(\omega_1 - \omega_2 - \omega_3 + \omega_4) \end{aligned} \tag{14}$$

2.5 FFF *mathematical model*

In this regime the vehicle essentially behaves as an airplane, thus we can consider the common longitudinal aircraft model [14]. In addition to the body-axis equations, it is important to express the equations of motion in the wind axis, because the aerodynamic forces act in these axis and (V_{tot}, α) can be expressed in terms of u and w. This reference system is used for translational equations because angle of attack and velocity are either directly measurable or closed related to directly measurable quantities, while the body axis velocities (u, w) are not. The equations of motion take the form

$$\begin{aligned} \dot{V} &= \frac{1}{m}[-D + T_t\cos\alpha - mg\,(\cos\alpha\sin\theta - \sin\alpha\cos\theta)] \\ \dot{\alpha} &= \frac{1}{Vm}[-L - T_t\sin\alpha + mg(\cos\alpha\cos\theta + \sin\alpha\sin\theta)] + q \\ \dot{\theta} &= q \end{aligned} \tag{15}$$

The angles θ and α lie in the same vertical plane above the north-east plane (Fig. 7a), and their difference is the flight-path angle $\Gamma = \theta - \alpha$ (Fig. 7b). Under this definition and from the last equation of (14):

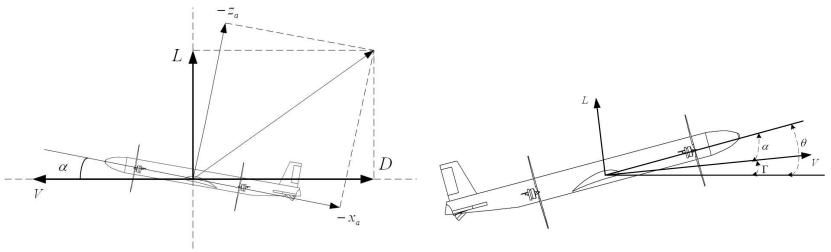

(a) Wind-Axis Reference Frame. (b) Flight-path angle definition.

Figure 7

$$\begin{aligned}
\dot{V} &= \frac{1}{m}[-D + T_t \cos\alpha - mg\sin\Gamma] \\
\dot{\alpha} &= \frac{1}{Vm}[-L - T_t \sin\alpha + mg\cos\Gamma] + q \\
\dot{\theta} &= q \\
\dot{q} &= \frac{1}{I_{yy}} M
\end{aligned} \tag{16}$$

3 Transition

The flight envelope of the vehicle encompasses different flight conditions, achieved by means of the collective angular displacement of the rotors. Indeed, is this tilting that provides a continuous mechanism to perform the operational transition. To illustrates this, let us consider the following scenario:

- $T_t >= mg$ i.e. The vehicle flies at a stabilized altitude
- $\theta \approx 0$ i.e. stabilized vertical flight

Is clear that as γ is tilted the horizontal velocity increases, while the altitude is reduced (Fig. 8 and 9). Thus, both vertical and horizontal controllers can still be used. For larger values of γ, i.e. $\gamma \approx> 45$, the vertical collective thrust is gradually reduced. The rotorcraft behaves more like a classical airplane. As the vehicle is gaining speed due to rotors tilt (γ), then

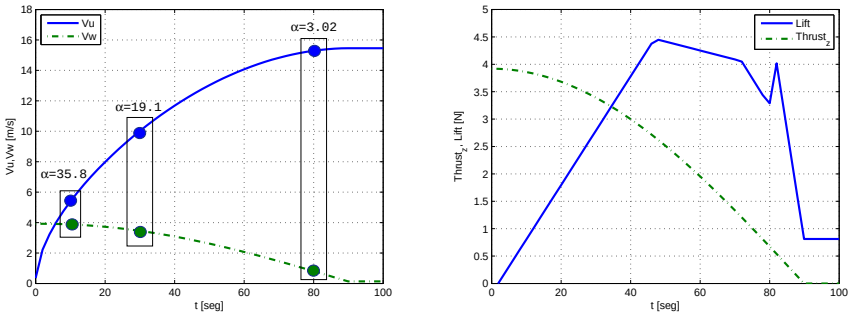

(a) Velocities V_u and V_w (b) Lift vs Thrust

Figure 8 Behavior of lift, thrust and velocities during the tilting of the rotors.

aerodynamic forces arise. For this reason we consider that the control of vertical and forward flight are active during the whole flight envelope.

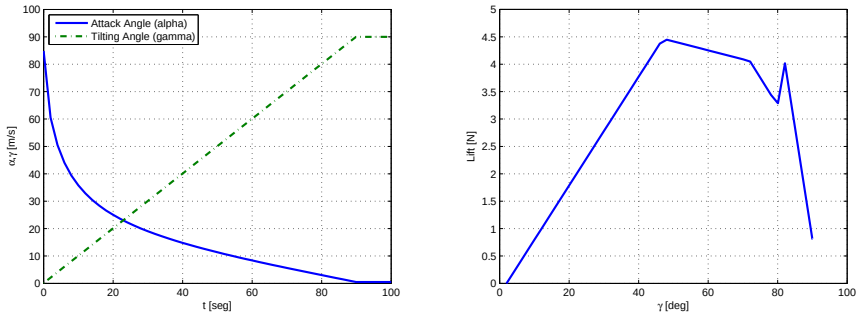

(a) α vs γ (b) Lift vs γ

Figure 9 The schema shows the behavior of lift, and angles γ and α during the tilting of the rotors.

4 Control strategy for hover flight mode

The vertical flight of the Quad-plane represents a challenging stage due to the aircraft's vertical dynamics are naturally unstable. In this regime, the Quad-plane aerial robot aims to emulate the flight behavior of a Quadrotor which features and non conventional Quadrotor design, i.e. an asymmetrical H-form structure.

Vertical flight regime encompasses two dynamic subsystems: the altitude dynamics, actuated by the thrust T , and the horizontal translational motion, generated by the pitch attitude. Taking into account the item 1) presented in section II, we can consider a simplified model from which is derived the controller in HF regime (i.e. $\alpha \approx 0$ since $\gamma = 0$).

For simplicity we consider that the gyroscopic moment is very small. These considerations allows us to rewrite (14) as

$$\begin{aligned} \ddot{X} &= -\left(\frac{T_{3,4}+T_{1,2}}{m}\right)(\sin\theta) \\ \ddot{Z} &= -\left(\frac{T_{3,4}+T_{1,2}}{m}\right)(\cos\theta) + g \\ \ddot{\theta} &= -\left(\frac{l_1}{I_{yy}}\right)(-T_{3,4}+T_{1,2}) \end{aligned} \tag{17}$$

If we rename the total thrust as $T_t = T_{3,4} + T_{1,2}$, and the difference of these thrusts as $T_d = T_{1,2} - T_{3,4}$. Then

$$\begin{aligned} \ddot{X} &= -\frac{T_t}{m}\sin\theta \\ \ddot{Z} &= -\frac{T_t}{m}\cos\theta + g \\ \ddot{\theta} &= -\frac{l_1}{I_{yy}}T_d \end{aligned} \tag{18}$$

thus, we have derived a simple model, suitable for controller design. The altitude (18b) can be stabilized via a feedback-linearizable input through

the total thrust T_t

$$T_t = -\frac{mu_z - mg}{\cos(\theta)} \tag{19}$$

where $u_z = -k_{p_z}(z - z^d) - k_{d_z}\dot{z}$ with $k_{p_z}, k_{d_z} > 0$ and z_d is the desired altitude. Since the vehicle works in an area close to $\theta \approx 0$, the singularity is avoided. For the subsystem 18a and 18c, a two-level hierarchical control scheme is used to stabilize its dynamics. The outer-loop control stabilizes the translational motion (slow dynamics [12]) along the x-axis, while the inner-loop control stabilizes the attitude (fast dynamics). Introducing (19) into (18a) and assuming that $z \approx z^d$, namely $u_z \to 0$, leads to

$$\ddot{x} \approx -g\tan\theta = -g\tan u_x \tag{20}$$

For the horizontal motion (20), θ can be considered as virtual control input u_x. However, it is a state not an actual control. Given that $\dot{\theta}^d$ is slowly time-varying, we will assume that the x-dynamics converges slower than the θ-dynamics. The reference for the inner-loop systems is

$$u_x = \theta^d = \arctan\left(\frac{-v_x}{g}\right) \tag{21}$$

$$\dot{u}_x = \dot{\theta}^d \approx 0 \tag{22}$$

where $v_x = k_{v_x}\dot{x} + k_{p_x}x$ with $k_{v_x}, k_{p_x} > 0$. Using the linearizing control input (21) in (20) yields

$$\ddot{x} = v_x, \text{ provided that } \tilde{\theta} = 0 \text{ (i.e. } \theta = \theta^d)$$

As the previous equation shows, the success of the outer-loop controller relies directly on the inner-loop attitude control performance, thus the inner loop controller must guarantee the stabilization of the attitude around the reference. For this reason, the stability analysis of the inner-loop controller is presented next. Consider the following positive function which is an unbounded function

$$V(\tilde{\theta}, \dot{\theta}) = \frac{1}{2}I_{yy}\dot{\theta}^2 + \ln(\cosh\tilde{\theta}) \tag{23}$$

Using (18) its corresponding time-derivative yields

$$\dot{V}(\tilde{\theta}, \dot{\theta}) = I_{yy}\dot{\theta}(-\frac{l_1}{I_{yy}}T_d) + \dot{\tilde{\theta}}\tanh\tilde{\theta} \tag{24}$$

Considering $\dot{\tilde{\theta}} = \dot{\theta}$, thus (24) may be rewritten as

$$\dot{V}(\tilde{\theta}, \dot{\theta}) = \dot{\theta}(-l_1 T_d + \tanh\tilde{\theta}) \tag{25}$$

Using the control input

$$T_d = \frac{\tanh\tilde{\theta} + \tanh\dot{\theta}}{l_1} \tag{26}$$

in (25) yields

$$\dot{V}(\tilde{\theta},\dot{\theta}) = -\dot{\theta}\tanh\dot{\theta}, \tag{27}$$

where $\dot{V}(\tilde{\theta},\dot{\theta}) \leq 0$. Therefore, the origin $(\tilde{\theta},\dot{\theta})$ is stable and the state vector remains bounded. The asymptotic stability analysis can be obtained from LaSalle's Theorem. Therefore, $\tilde{\theta} \to 0$ and $\dot{\theta} \to 0$ as $t \to \infty$.

5 Control strategy for forward flight mode

In this section the flight path angle Γ will be controlled using the *backstepping* algorithm taking the following approximations into consideration:

- The air speed is assumed constant, $\dot{V} = 0$ [15].
- From the definition of flight-path angle, the dynamics $\dot{\Gamma} = \dot{\theta} - \dot{\alpha}$ yields $\dot{\Gamma} = \frac{1}{mV}[T_t \sin\alpha + L - mg\cos\Gamma]$.
- The thrust term $T_t \sin\alpha$ in (16) will be neglected as it is generally much smaller than lift.
- $C_m = C_{m_\delta}(\alpha)\delta$, since the main contribution to M is provided by the elevator.

With these considerations in mind and using the change of coordinates $\zeta = \Gamma - 1/2\pi$, the system (16) may be expressed as

$$\begin{aligned}
\dot{\zeta} &= -\frac{g\cos(z+1/2\pi)}{V} + \frac{C_{l_\alpha}\alpha}{mV} \\
\dot{\alpha} &= \frac{g\cos(z+1/2\pi)}{V} - \frac{C_{l_\alpha}\alpha}{mV} + q \\
\dot{q} &= \frac{1}{I_{yy}} C_{m_\delta}\delta
\end{aligned} \tag{28}$$

Equation (29) is now in *feed forward* form for *backstepping* procedure. For notational simplification, let

$$\begin{aligned}
\dot{x} &= f(x) + \xi_1 \\
\dot{\xi}_1 &= f_1(x,\xi_1) + \xi_2 \\
\dot{\xi}_2 &= f_2 + g_2(\xi_1)u
\end{aligned} \tag{29}$$

with

$$\begin{array}{rcl|rcl}
x &=& \frac{mV\Gamma}{C_{l_\alpha}}; & f(x) &=& -\frac{g}{V}\cos\left(\frac{C_{l_\alpha}x}{mV}\right) \\
\xi_1 &=& \alpha; & f_1(x,\xi_1) &=& \frac{g}{V}\cos\left(\frac{C_{l_\alpha}x}{mV}\right) - \frac{C_{l_\alpha}\xi_1}{mV} \\
\xi_2 &=& q; & f_2 &=& 0 \\
u &=& \delta; & g_2(\xi_1) &=& \frac{1}{J_y}C_{m_\delta}
\end{array} \tag{30}$$

Defining the following error states as

$$\begin{aligned}
e &\triangleq x - x_{des} \\
e_1 &\triangleq \xi_1 - \xi_{1,des} \\
e_2 &\triangleq \xi_2 - \xi_{2,des}
\end{aligned} \tag{31}$$

Now, following the backstepping procedure differentiating the first equation in (31) yields

$$\dot{e} = f(x) + \xi_{1,des} + e_1 - \dot{x}_{des} \tag{32}$$

where $\xi_{1,des}$ is viewed as a virtual control for the last equation, choosing as $\xi_{1,des} = -f(x) - k_1 e + \dot{x}_{des}$. Then substituting this virtual control in (32) we have that

$$\dot{e} = -ke + e_1 \tag{33}$$

Repeating the same procedure, differentiating e_1 yields

$$\dot{e}_1 = f_1(x, \xi_1) + e_2 + \xi_{2,des} - \dot{\xi}_{1,des} \tag{34}$$

Let $\xi_{2,des} = -f_1(x, \xi_1) - e - k_1 e_1 + \dot{\xi}_{1,des}$ so that

$$\dot{e}_1 = -e - k_1 e_1 + e_2 \tag{35}$$

As a last step, now the real control signal is obtained in similar way. Differentiating e_2 yields

$$\dot{e}_2 = f_2 + g_2(\xi_1)u - \dot{\xi}_{2,des} \tag{36}$$

Let

$$u = \frac{1}{g_2(\xi_1)} \left[-f_2 - e_1 - k_2 e_2 + \dot{\xi}_{2,des} \right] = u(\dddot{z}_d, \ddot{z}_d, \dot{z}_d, z_d, e, e_1, e_2) \tag{37}$$

so that

$$\dot{e}_2 = -e_1 - k_2 e_2 \tag{38}$$

It is important to ensure that $g_2(\xi_1) \neq 0$, which occurs only with big enough negative values of α. These values are assumed to be impossible to achieve in standard operation of the airplane, so avoiding division by zero. Equations (33,35,38) expressed in vectorial form

$$\dot{\mathbf{e}} = -K\mathbf{e} + S\mathbf{e} \tag{39}$$

we can see that $S = -S^T$ satisfies $\mathbf{e}^T S\mathbf{e} = 0, \forall \mathbf{e}$, so that with the Lyapunov-candidate-function $V(\mathbf{e}) = \frac{1}{2}\mathbf{e}^T\mathbf{e}$, and the time derivative evaluated in the trajectories yields

$$\dot{V}(\mathbf{e}) = \mathbf{e}^T(-K\mathbf{e} + S\mathbf{e}) = -\mathbf{e}^T K\mathbf{e} < 0, \forall \mathbf{e} \tag{40}$$

This proves that the above differential equation, is asymptotically stable about the origin.

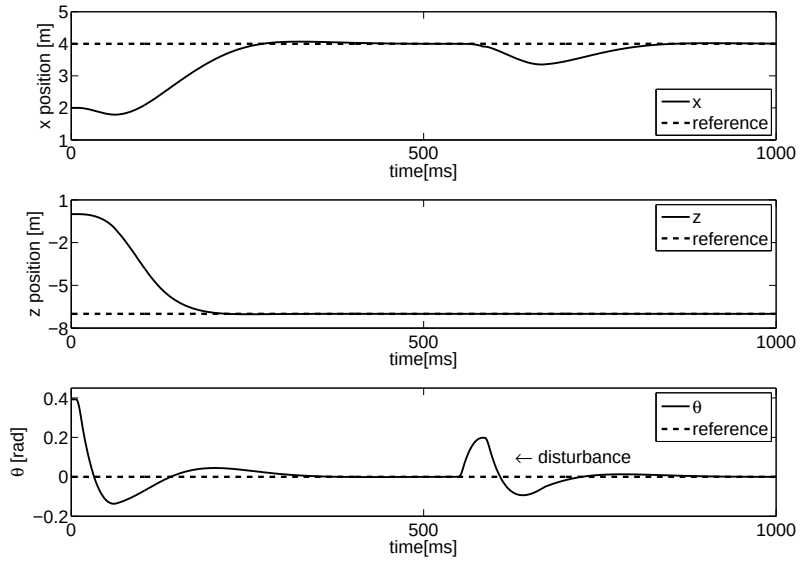

Figure 10 Position and attitude of the vehicle under disturbance condition.

6 Simulation results

6.1 HF

The performance of the nonlinear controller presented in the previous section is evaluated on the dynamic model (18) in MATLAB/Simulink. We started the Quad-plane at the position $(x_0, z_0, \theta_0) = (2, 0, \frac{\pi}{8})$ and $(\dot{x}, \dot{z}, \dot{\theta}) = (0, 0, 0)$. The aircraft had the task of performing hover flight at $(x^d, z^d, \theta^d) = (4, -7, 0)$. Figures 10 and 11 show the evolution and convergence of the states $(x, \dot{x}, z, \dot{z}, \theta, \dot{\theta})$ to the desired references with the initial conditions mentioned above. It is important to note that position and angle references are tracked with negligible steady state errors. The controller is robust in the presence of a perturbation in $t = 600$ ms with a magnitude of $1/8\pi$ radians, as seen in figures 10 and 11. Table 1 shows the real parameters for simulation analysis.

The control inputs are depicted in the figure 12, which shows the reaction to the disturbance.

6.2 FFF

After the vehicle experiments the transition-flight, its behavior is like an airplane. We have considered the next initial conditions for purposes of simulation $\Gamma_0 = 5$, $\alpha_0 = 5$ and $\theta_0 = 10$. The aircraft had the task of

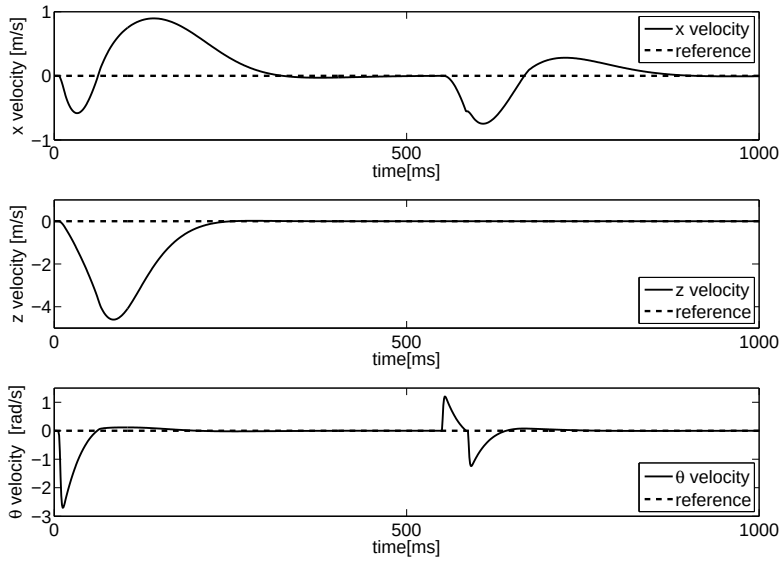

Figure 11 Derivatives of the position and attitude of the vehicle under disturbance condition.

tracking a trajectory shown in the first part of Fig. 13. This figure shows the evolution and tracking trajectory of the states $(\Gamma, \alpha, z, \theta)$ to the desired reference with the initial conditions mentioned above. It is important to note that angle references are tracked with negligible steady state errors.

7 Experimental setup

The goal of this section is to present an experimental autonomous hover flight to evaluate not only the performance and reliability of the proposed concept but also the efficacy of the proposed control algorithm. We have programmed a ground station in MATLAB/Simulink for on-line variable monitoring/adjusting.

7.1 Onboard flight system (OFS)

1. *Experimental prototype:*
   The vehicle's fuselage and the H-form structure are built of carbon fiber and balsa wood (Fig. 1). The wing was built with depron. Four counter rotating and tilting brushless motors provide the thrust, while the tilting mechanism of the engines is controlled through two analog servomotors.

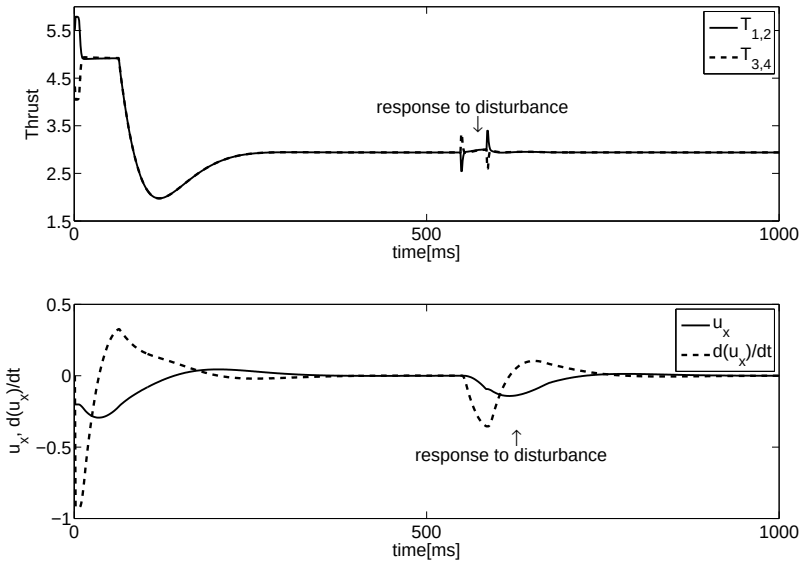

Figure 12 UAV's control inputs and response to disturbance.

Parameter	Value
mass (m)	$0.8kg$
gravity (g)	$9.8\frac{m}{s^2}$
$\bar{C}$	$0.2m$
l_1	$0.25m$
Wing span	$1.15m$

Table 1 Parameters.

2. *Flight control CPU:*
The attitude control algorithm is implemented on the TMS320F2808 digital signal processor (DSP) (Fig. 15) which is highly integrated, high-performance solutions for demanding control applications. It has a high-Performance 32-Bit CPU at 100Mhz and 128K x 16 of embedded flash memory. This DSP is notable for its rich set of on-chip peripherals including three 32-bit CPU-Timers, two event-manager modules (EVA, EVB), PWM, capture,enhanced analog-to-digital converter (ADC) module, I2C module, serial communications interface modules (SCI-A, SCI-B), serial peripheral interface (SPI) module, digital I/O and shared pin functions and watchdog. The I2C is used to control the four rotors via YGE30i brushless controller and to read the magnetic compass CMPS03, two PWM outputs are used to control the tilting mechanism, the (ADC) module is used to communicate the Homemade IMU with the DSP. The

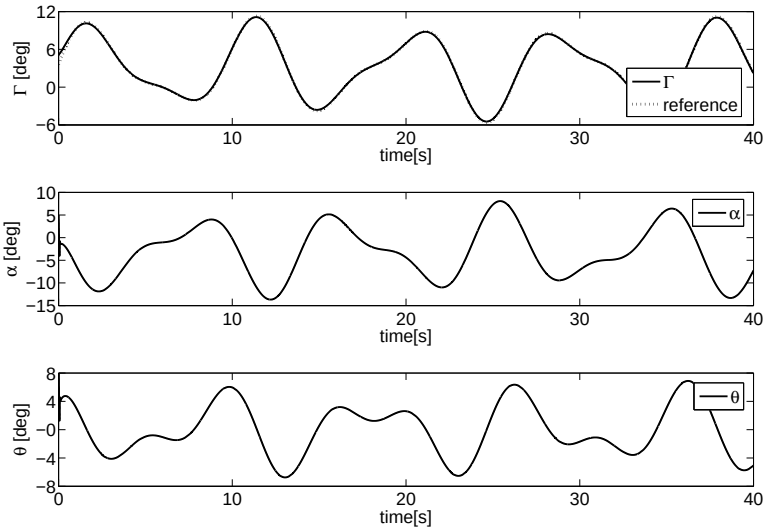

Figure 13 Trajectory tracking.

wireless communication between Quad-plane and the ground station is performed through a wireless serial protocol (two X-bee pro modems). One input capture acquires the RC-PPM (Pulse Position Modulated) signal from the radio, which is used only to set the initial attitude and to provide the gas by the user. With the fast response of the combination YGE30i brushless controller and the Robbe Roxxy motor, we can set the execution time for each iteration loop to be 2ms.

3. *Homemade IMU:*
   The homemade inertial measurement unit (IMU) (Fig. 15) is composed of three accelerometers and three gyroscopes, measuring the angular position and rate along the three axis of the inertial frame. The comunnication between the homemade IMU and the DSP is with the ADC module of the DSP.

7.2 Experimental results

The figures 16, 17 and 18, shows the experimental attitude performance of the vehicle during the vertical flight. As we can see in the pictures, the vehicle was perturbed, and the states remains bounded.

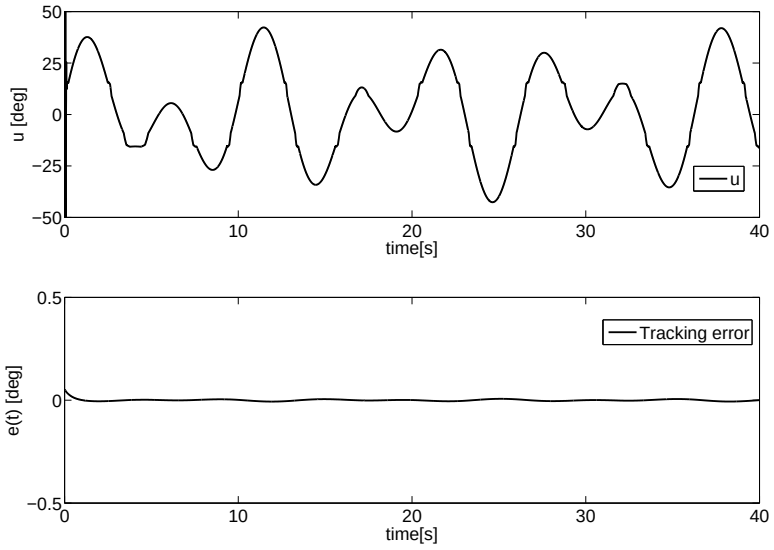

Figure 14 Control and error defined by $e = \Gamma - \Gamma_d$.

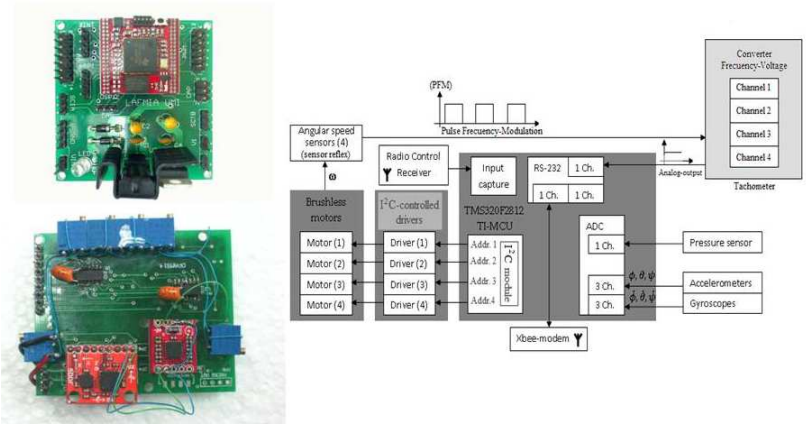

Figure 15 Homemade IMU, DSP-based embedded flight system and working principle of the Quad-plane UAV system.

8 Concluding remarks and future work

This paper describes an experimental convertible aircraft that is under development at the Compiègne University.

The longitudinal dynamics of this aircraft including its aerodynamics are derived at the hover and forward flight operating mode. The proposed control strategies were evaluated, at simulation level, for the nonlinear dynamic

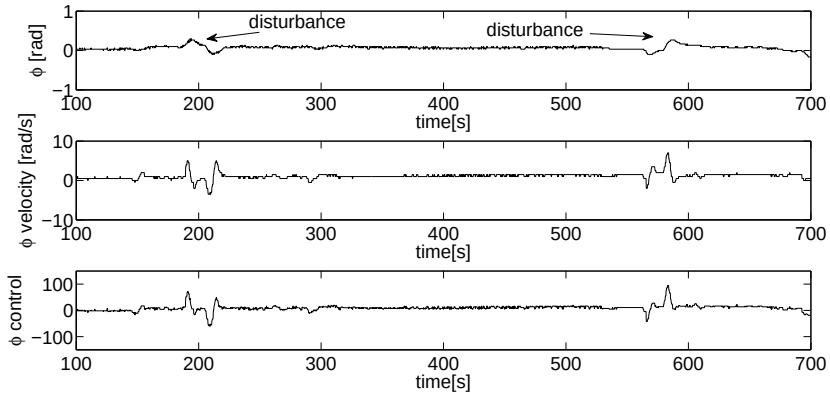

Figure 16 Roll behavior in the automatic hovering flight test.

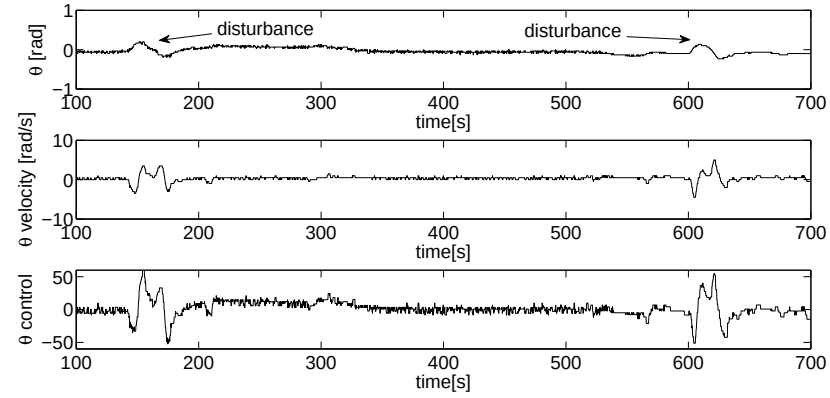

Figure 17 Pitch behavior in the automatic hovering flight test.

model, obtaining satisfactory results. The angular position and velocity are obtained through an onboard IMU. A DSP-based embedded flight system was designed and built to implement an attitude controller law. The proposed control algorithm is based on an inner-outer loop scheme since it is suitable for implementation purposes.

An experimental setup (prototype and EFCS) was designed to perform an autonomous attitude-stabilized flight in hover regime showing a relevant performance in presence of external disturbances. Future work includes the transition flight between cruise and hover flight modes (transition flight) to evaluate the accuracy of the model and to validate the control algorithm.

For energy-saving purposes during forward flight (airplane mode), it is proposed that the vehicle can lead its orientation towards wind velocity vector. To achieve this objective, the vehicle could easily rotate its orientation

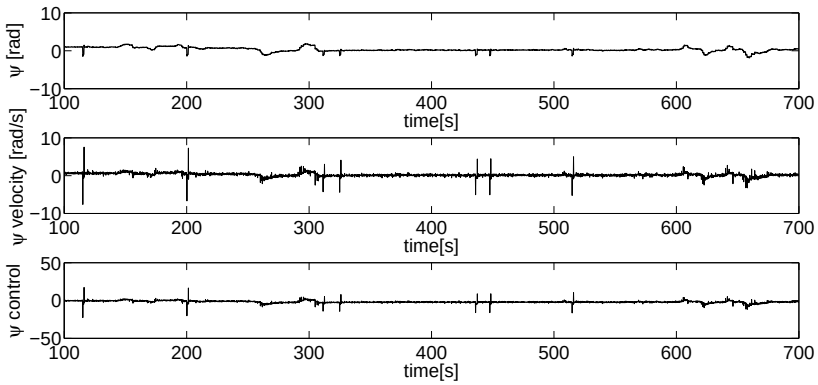

Figure 18 Yaw behavior in the automatic hovering flight test.

(yaw movement in helicopter mode) and once addressed the wind vector, switch to airplane mode. In the proposed configuration, this process could be quite simple, since the vehicle is always maintained with the roll and pitch angles close to zero, which is not possible in the case of a tail-sitter configuration since within vertical mode the wing surface is highly vulnerable to wind gusts. It is possible to asses with a gyro-stabilized camera in order to record and send images and video of the inspection area without loss of the target to be captured. Again, this would be more complex for a tail-sitter configuration, due to the difference of 90 degrees between the two flight modes. A video showing the robust performance of the vehicle in hover mode is available at: http://www.youtube.com/watch?v=S9xCDrGPSG0

References

1. R. Hugh Stone, Control Architecture for a Tail-sitter Unmanned Air Vehicle, *5th Asian Control Conference*, Melbourne, Australia, July 23-25, 2004.
2. J. Escareño, H.R. Stone, A. Sanchez and R. Lozano, Modeling and Control Strategyfor the transition of a Convertible UAV, *European Control Conference (ECC07)*, Kos, Greece, 2007.
3. H. Stone, Aerodynamic Modeling of a Wing-in-Slipstream Tail-Sitter UAV, *Biennial International Powered Lift Conference and Exhibit*, Williamsburg, Virginia, Nov. 5-7, 2002.
4. William E. Green and Paul Y. Oh, Autonomous Hovering of a Fixed-Wing Micro Air Vehicle, *International Conference on Robotics and Automation*, Orlando, Florida, USA, May, 2006.
5. J. Escareno, S. Salazar and R. Lozano, Modeling and Control of a Convertible VTOL Aircraft, *45th IEEE Conference on Decision and Control*, San Diego, California, December 13-15, 2006.
6. A. Bedford, and W. Fowler, *Dynamics*, Addison-Wesley Publishing Company, 1989.
7. B. Etkin and L. Reid, *Dynamics of Flight*, J. Wiley & Sons, Inc., 1991.

8. B. L. Stevens and F.L. Lewis, *Aircraft Control and Simulation 2ed.*, J. Wiley & Sons, Inc., 2003.
9. Snyder, D., The Quad Tiltrotor: Its Beginning and Evolution, Proceedings of the 56th Annual Forum, American Helicopter Society, Virginia Beach, Virginia, May 2000.
10. K. Nonami, Prospect and Recent Research and Development for Civil Use Autonomous Unmanned Aircraft as UAV and MAV, Journal of System Design and Dynamics, **Vol.1, No.2,** 2007.
11. Kaan T. Oner, Ertugrul Cetinsoy, Mustafa Unel, Mahmut F. Aksit, Ilyas Kandemir y Kayhan Gulez. Dynamic Model and Control of a New Quadrotor Unmanned Aerial Vehicle with Tilt-Wing Mechanism, World Academy of Science, Engineering and Technology 45 2008.
12. Peter V. Kokotovic, John O'Reilly y Hassan K. Khalil, *Singular Perturbation Methods in Control: Analysis and Design*, Academic Press, 1986.
13. Stengel, R., *Flight Dynamics*, Princeton University Press, 2004.
14. Brian L. Stevens y Frank L. Lewis, *Aircraft Control and Simulation*, John Wiley and Sons Inc, 1992.
15. Declan Mates, Martin Hagstrom. *Nonlinear Analysis and Synthesis Techniques for Aircraft Control*. Lecture Notes in Control and Information Sciences 365. Springer 2007.